Gas hydrate in the North Carnarvon Basin, offshore Western Australia

Fawz Naim[a], Ann E. Cook[a]

[a] School of Earth Sciences, The Ohio State University, Columbus, OH, USA

Corresponding author: Fawz Naim (naim.9@buckeyemail.osu.edu)

Abstract

Analysis of hydrate systems across basins is not common, as most studies are focused on smaller sites. Using petroleum industry well and seismic data, we identify natural gas hydrate accumulations across the entire North Carnarvon Basin, offshore Western Australia. Out of 120 wells, 52 wells have evidence for gas hydrate, though hydrate is distributed throughout the hydrate stability zone in low concentrations. In addition, we do not observe a connection between the presence of hydrate in wells and deeper thermogenic gas reservoirs. From 3D seismic data, we observe bottom simulating reflections (BSRs) are very rare. In addition, while faults are common across the basin, shallow bright spots, which indicate shallow free gas, are uncommon. Based on all these observations from well and seismic data, we argue that hydrate across the North Carnarvon Basin formed predominantly from in-situ gas that is microbial in nature.

Keywords: Gas hydrate, well logs, seismic, bottom simulating reflection

1. Introduction

Natural gas hydrate commonly occurs on continental slopes within marine sediments (Collett et al., 2009). Identifying and characterizing natural gas hydrate is important for several reasons. Hydrate can be a potential geohazard as hydrate dissociation may trigger underwater landslides. Hydrate is also a potential natural gas resource that hosts vast quantities of methane (Boswell & Collett, 2011; Collett et al., 2009; Maslin et al., 2010). Moreover, hydrate is also an important component of the global carbon cycle as it is estimated to host ~5-20% of mobile carbon on Earth (Boswell & Collett, 2011; Ruppel & Kessler, 2017). Understanding the source of gas in hydrate systems – either microbial or thermogenic gas – may help us understand the role of hydrate in the global carbon cycle (Kvenvolden, 1988, 2002). Microbial gas is formed from the consumption of organic matter by microorganisms in near seafloor sediments, while thermogenic gas is formed from the degradation of organic matter under high temperature and pressure conditions occurring far below the seafloor (Brooks et al., 1984; Kvenvolden, 2002). Characterizing the gas source for hydrate systems will help us understand the migration of gas and the formation and accumulation of hydrate in near seafloor systems.

Several countries such as Japan, Canada, China, India, Korea and the U.S. have conducted studies to drill and identify gas hydrate, but these studies only focus on relatively small areas (Collett et al., 2009; Collett et al., 2014; Fujii et al., 2014; Hui et al., 2016; Ryu et al., 2009; Takahashi et al., 2005; Tsuji et al., 2009). The occurrence and distribution of hydrate across larger basins, however, is still not well understood. For example, the largest hydrate study offshore Western Australia, Paganoni et al. (2019) is focused on natural gas hydrate in the North Carnarvon Basin, offshore Western Australia (white polygon, Figure 1); while the Paganoni study included 4130 km^2 of 3D seismic data, it covers only a small fraction (0.8%) of the North Carnarvon Basin. Herein, we identify the presence of natural gas hydrate for the first time on a wide scale across the North Carnarvon Basin in offshore Western Australia using petroleum industry reflection seismic data and downhole well logs, which covers an area of 34,000 km^2 (Figure 1).

The two most common geophysical methods used to identify natural gas hydrate are downhole logging and reflection seismic surveys (Goldberg et al., 2010; Holbrook et al., 1996). Downhole logs provide a variety of physical properties measurements, which can be used to determine the in situ characteristics of hydrate and hydrate saturation (Goldberg et al., 2010; Tsuji et al., 2009). The most common downhole logs for interpreting hydrate are bulk density, resistivity and compressional velocity (Goldberg et al., 2010). Bulk density provides the most accurate measurement of porosity in the hydrate stability zone (HSZ), which is essential for interpreting hydrate using both resistivity and compressional velocity (Helgerud et al., 1999; Lee & Collett, 2011). Hydrate is an electrical insulator and increases electrical resistivity even if it is present in small amounts. Compressional velocity increases in hydrate bearing intervals when hydrate saturation is above ~40% (Yun et al., 2005).

Marine reflection seismic data are used to interpret hydrate systems and free gas. . Seismic data is often used to identify bottom simulating reflections (BSRs) which occur due to the presence of free gas at the base of hydrate stability zone (BHSZ) (Haacke et al., 2007; Shipley et al., 1979), but BSRs do not always indicate hydrate (Majumdar et al., 2016). In some cases, phase reversals may be present at or near the BSR, which can be a direct hydrate indicator on seismic data (Bellefleur et al., 2007; Boswell et al., 2016; Collett et al., 2019). Free gas can also be associated with bright spots, chimneys and faults (Heggland, 1998; Hillman et al., 2020; Ligtenberg, 2003; Miller et al., 2012; Sheriff, 1975). Bright spots are high amplitude anomalies with a negative acoustic impedance that indicates the presence of natural gas (Sheriff, 1975). Gas chimneys are often identified by low amplitude anomalies on seismic data; these features can extend deep into the subsurface (Heggland, 1998). Faults appear as discontinuities with offsets in stratigraphy and can be both shallow or deep seated. Faults can also be highly permeable and gas migration from deep reservoirs can occur along such migration pathways (Miller et al., 2012).

1.1 Hydrate systems in the North Carnarvon Basin

Most of the sediments within the HSZ in the North Carnarvon Basin are part of the Delambre Formation, which consists primarily of nannofossil carbonate ooze (Barrett et al., 2021; Bradshaw et al., 1994). At Site 762 and 763 from Ocean Drilling Program (ODP) Leg 122, (Figure 1) the total carbonate content of the sediments ranges from 60-80% from 0-400 mbsf (meters below seafloor) (Haq et al., 1990). Moreover, in shallow shelf sediments the lithology primarily consist of unconsolidated wackestone and packstone at International Ocean Discovery Program (IODP) Sites U1461, U1462, U1463 (Figure 1; Gallagher et al., 2017). This shows that carbonate is widely deposited in the shallow sediments within the Exmouth Plateau.

Only a few studies describe the presence of hydrate offshore Western Australia. Imbert & Ho (2012) inferred the presence of hydrate from the observation of funnel shaped features from a seismic survey in the Exmouth Plateau. The study by Imbert & Ho (2012) however, does not present any direct evidence (such as well logs and geochemical data) for the presence of hydrate. Similarly, Paganoni et al. (2019) inferred the presence of hydrate system in the Exmouth Plateau in offshore Western Australia using the 3D Bonaventure seismic survey and geochemical data from ODP Sites 762 and 763 (Figure 1).

In the Bonaventure survey, Paganoni et al. (2019) identified a few discontinuous BSR-like features that are negative amplitude anomalies that most likely signify the presence of free gas at and below the reflection and possible gas hydrate occurring above. These BSR-like features, however, are difficult to interpret due to the presence of sedimentary layers that are parallel to the seafloor. In the seismic data, Paganoni et al., (2019) also observed a dense network polygonal faults, which may act as potential conduits for gas migration (Cartwright et al., 2003; Cartwright & Lonergan, 1997) in the Exmouth Plateau in offshore Western Australia.

Based on the seismic interpretation and geochemical data below the HSZ from industry boreholes in the Exmouth Plateau, Paganoni et al., (2019) inferred the presence of a hydrate system sourced with thermogenic gas from deep gas reservoirs, most likely the Mungaroo formation in the Upper Triassic. Paganoni et al. (2019) suggested that the gas has likely migrated through faults and stratal pathways that is evident from the presence of stacked high amplitude anomalies and gas chimneys on seismic data.

1.2 The Petroleum System in the North Carnarvon Basin

The North Carnarvon Basin has ~46 trillion cubic feet of proved and probable oil and gas reserves making it the highest hydrocarbon producing region in Australia (Geoscience Australia, 2022). The main source rocks in the North Carnarvon Basin comprise of the Upper Triassic Mungaroo Formation with some contribution from organic rich marine units from the Lower Triassic Locker Shale (Bradshaw et al., 1994). The reservoir bearing rocks in the North Carnarvon Basin consist of sand-prone facies of the Triassic Mungaroo Formation and Barrow Group in the Early Cretaceous (Exon & Willcox, 1980; Geoscience Australia, 2022). Hydrocarbon leakage from the Triassic Mungaroo Formation into shallow sediments could be a thermogenic source for hydrate (e.g. Scarborough gas field) (Cowley & O'Brien, 2000).

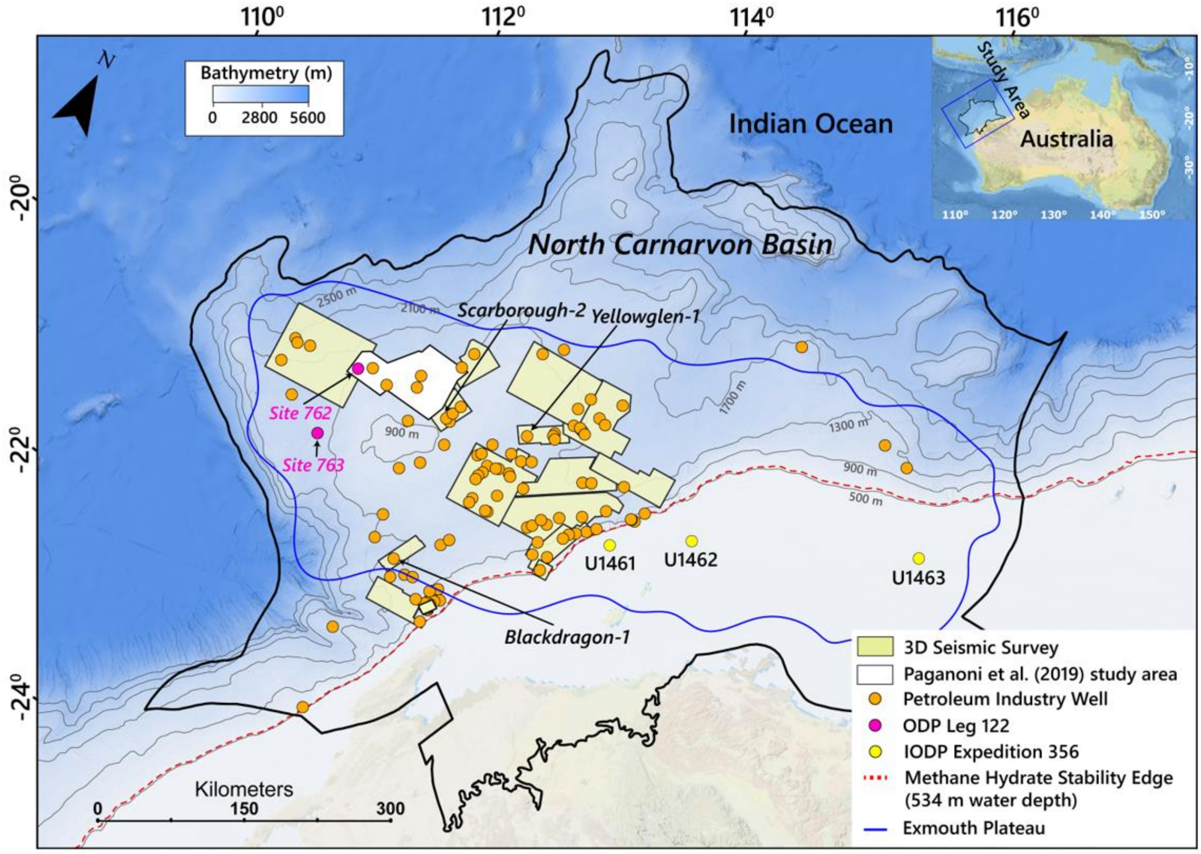

Figure 1 A map showing the data used to characterize hydrate systems in the North Carnarvon Basin, offshore Western Australia. The orange dots are the petroleum industry wells evaluated in this study; the pink dots are ODP (Ocean Drilling Program) Sites 762 and 763; the yellow dots are the IODP (International Ocean Discovery Program) Sites U1461, U1462 and U1463. Seismic surveys interpreted in this study are shown as yellow shaded areas. The white shaded area is the Bonaventure 3D seismic survey used by Paganoni et al. (2019), as well as in this study.

There is also evidence for microbial methane sources at ODP Sites 762 and 763 (Figure 1). Hydrocarbon data from these sites show high methane concentrations up to 100,000 ppm in headspace gas samples (Snowdon & Meyers, 1992), which may suggest a microbial methane source (Claypool & Kvenvolden, 1983). The measured total organic carbon (TOC) at Site 762 is quite low, less than 1%. At Site 763, most TOC measurements are between 0.2-1.5%. While these values are low, low methane and low hydrate concentrations can be generated from small amounts of organic carbon (e.g. Malinverno, 2010). In addition, extremely high TOC ranging from 9-15% in two thin (3 cm and 10 cm) layers at Site 763 are significant TOC sources for microbial gas generation (Figure 1) (Haq et al., 1990; Snowdon & Meyers, 1992).

2. Data and Methods

We use water column temperature, petroleum industry wells and 3D seismic surveys from the National Oceanic and Atmospheric Administration (NOAA), the National Offshore Petroleum Information Management System (NOPIMS), and the Western Australian Petroleum and Geothermal Information Management System (WAPIMS). NOPIMS and WAPIMS provide public access to the petroleum exploration data from Australia in the form of well logs, marine seismic surveys, interactive maps, and cores.

2.1 Estimating the Base of Hydrate Stability Zone

Hydrate stability below the seafloor depends on temperature, pressure, pore water salinity and gas composition (Sloan & Koh, 2007). We use the Colorado School of Mines Hydrate CSMHYD program (Sloan & Koh, 2007) to estimate the BHSZ in each well using the water depth, the seafloor temperature and the geothermal gradient at each well location. (These datasets are available in the Supplementary_Material spreadsheet). We assume 100% methane (Structure I) and 3.5% porewater salinity to estimate the BHSZ. We assume methane gas because most hydrate accumulations worldwide predominantly consist of methane gas (Ruppel & Kessler, 2017; Sloan & Koh, 2007). In addition, the methane concentration from the gas chromatograph data in the petroleum industry wells in North Carnarvon Basin increases to 99% from deeper to shallower sediments indicating predominantly methane gas in hydrate. Also, it has been found that the gas hydrate reservoir at Green Canyon Block 955 in the Gulf of Mexico is composed almost entirely of microbial methane (99.99%) that was expected to have a thermogenic source with higher order hydrocarbons (Flemings et al., 2020; Phillips et al., 2020).

We use well completion reports from the NOPIMS and WAPIMS databases to determine the water column depth at each wellhead. There are ~1600 wells drilled in offshore Western Australia with water depths ranging from the continental shelf to deep water settings. However, we only use wells with water depths > 534 m, because the up dip edge of methane hydrate stability in offshore Western Australia is ~534 m based on our calculations using the CSMHYD program (Sloan & Koh, 2007).

Seafloor temperature is needed to estimate the geothermal gradient and calculate the BHSZ. We use the deepest available water column temperature data from the World Ocean Atlas (Boyer et al., 2018; Locarnini et al., 2018) to estimate the seafloor temperature at each well (Boyer et al., 2018; Locarnini et al., 2018).

To estimate the geothermal gradient, a temperature measurement below the seafloor is also needed. In industry wells, formation pressure tests provide the most precise estimate of formation temperature below the seafloor (Anderson et al., 2011). Formation pressure tests are conducted by packing a specific interval in the borehole, which allows the borehole fluids to reach equilibrium with the formation so that the formation temperature can be measured (Peters & Nelson, 2012). In our dataset, 81 wells have formation pressure test data and we use this data to compute the geothermal gradient at those wells.

Another type of temperature measurement is the bottomhole temperature (BHT); this measurement is the maximum recorded temperature inside the borehole at the bottom of the hole. BHT measurements may be less reliable than the formation pressure tests, because BHT measures the temperature of drilling fluid at the bottom hole and that temperature may not be equal to the temperature of the formation (Evans & Coleman, 1974). In our dataset, 24 wells have formation pressure test in addition to BHT data, which provides an opportunity to compare the similarity between the two temperature measurements. We find that the mean absolute difference was 1.85 C/km with the maximum difference of +8.04 C/km and minimum difference of +0.17 C/km, where the positive sign indicates a warmer gradient from the formation pressure test data. Because the mean difference between the formation pressure test and BHT gradients was low, we argue that BHT is a reliable estimate of the geothermal gradient in wells where no formation pressure test data was available. Therefore, we use BHT to estimate BHSZ for 38 wells with no formation pressure test measurements.

For the remaining 27 wells with no BHT and formation pressure test data, we estimate the geothermal gradient using the weighted average geothermal gradient from other wells within a radius of 70 km.

2.2 Gas Hydrate Interpretation

Once we estimate the BHSZ, we choose wells with at least 30 m of valid well log data within the HSZ for interpretation. We also eliminate data that is poor quality. For example, metal casing generates inaccurate or erratic resistivity that can be easily identified and removed.

We use gamma ray and resistivity logs for interpreting sediment type and hydrate occurrence as these logs are most commonly available within the HSZ for these wells. If other logs are available within the HSZ, such as bulk density and compressional velocity, they are also used to interpret the lithology and hydrate occurrence.

Resistivity logs are used to identify gas hydrate and estimate background resistivity. Background resistivity is the resistivity of sediments that are 100% saturated with brine-rich water. As the hydrate displaces pore fluid in the pore space, the measured resistivity increases (Goldberg et al., 2010). We interpret this increase in resistivity with reference to the background resistivity to identify hydrate saturated intervals (Goldberg et al., 2010; Pearson et al., 1983).

Background resistivity can either be calculated or estimated depending on the type and quality of logs available in a well. Background resistivity can be calculated when a quality bulk density log and resistivity log are available. A bulk density log is used to compute porosity as it provides the most accurate porosity in near seafloor sediments (Goldberg et al., 2010). We show an example in Figure 2 where we compute porosity using a bulk density log for the Yellowglen-1 well. We assume a typical grain density (ρ_g) for of 2.70 g/cm^3 for carbonate sediment and a fluid density (ρ_f) of 1.03 g/cm^3 for brine-rich porewater:

$$\phi_{den} = \frac{\rho_g - \rho_b}{\rho_g - \rho_w} \quad (1)$$

The ϕ_{den} porosity calculated from Equation (1) can then be used to compute the background resistivity R_o using the Archie's equation (Archie, 1942):

$$R_o = \frac{R_w}{\phi^m} \quad (2)$$

where R_w is the pore water resistivity and is assumed to be the resistivity of seawater, R_w = 0.32 Ωm (Ellis & Singer, 2007). The cementation exponent (m) is related to the cementation of sediment (Ellis & Singer, 2007). We use the value m=2 initially for the complete interval and adjusted it to 2.4 for the interval 1365 to 1407 mKB and 2.2 for the interval below 1407 mKB to match R_o in water saturated intervals for the Yellowglen-1 well in Figure 2 (Ellis & Singer, 2007).

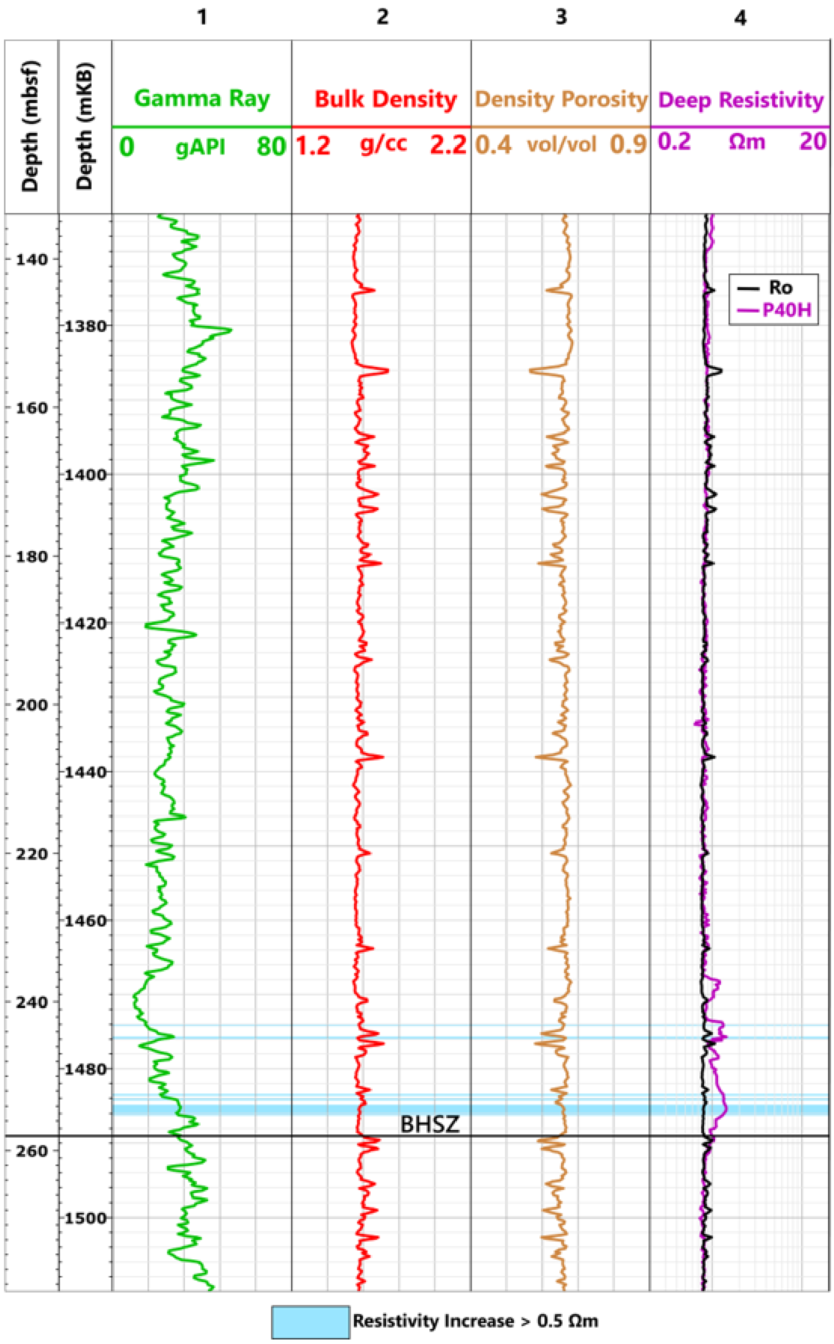

Figure 2 Well log data from Yellowglen-1. The first depth track is the depth in meters below seafloor (mbsf). The second depth track is the depth as measured in meters from the Kelly Bushing (or rig floor). Track 1 displays the gamma ray log that shows the variation in lithology with depth; the low gamma ray suggests the sediment consists primarily of carbonate ooze. Track 2 shows the original bulk density (in red). Track 3 displays the porosity calculated using Equation (1). Track 4 shows the deep resistivity (P40H, in purple) and background resistivity (R_o) calculated using Equation (2). Other propagation resistivity logs also agree with the P40H log and do not show any deviations from P40H in the HSZ. The base of hydrate stability is estimated based on the geothermal gradient (46.6 C/km) from formation pressure tests. The highlighted intervals (light blue) show resistivity increases greater than 0.5 Ωm with reference to the computed R_o. These highlighted intervals are categorized as hydrate bearing and the well is Category D hydrate.

In the wells where bulk density log is not available, we estimate R_o. Usually, R_o varies between 1-1.5 Ωm for water-saturated near seafloor sediments, due to changes in porosity. We choose a conservative R_o to avoid overestimating the presence of hydrate in the wells. We observe the resistivity trend all throughout the HSZ, as well as at and just below BHSZ to select the most likely R_o. R_o can increase with depth due to decreasing porosity because of compaction. In such cases where R_o is variable, different R_o values are chosen for different intervals. For example, in Blackdragon-1 (Figure 3) we select a R_o of 1 Ωm from 1429 -1636 mKB, 1.2 Ωm from 1636 - 1691 mKB, and 1.4 Ωm below 1691 mKB.

Gas hydrate saturation is using Archie's saturation equation (Archie, 1942) :

$$S_h = 1 - \left(\frac{R_o}{R_m}\right)^{1/n} \qquad (3)$$

where R_o is the calculated background resistivity using Equation 2, R_m is the measured resistivity and n is the saturation exponent (for example Scarborough-2, Figure 4). However, caution should be taken while using Archie's equation as it should only be applied where hydrate is present in the primary pore space.

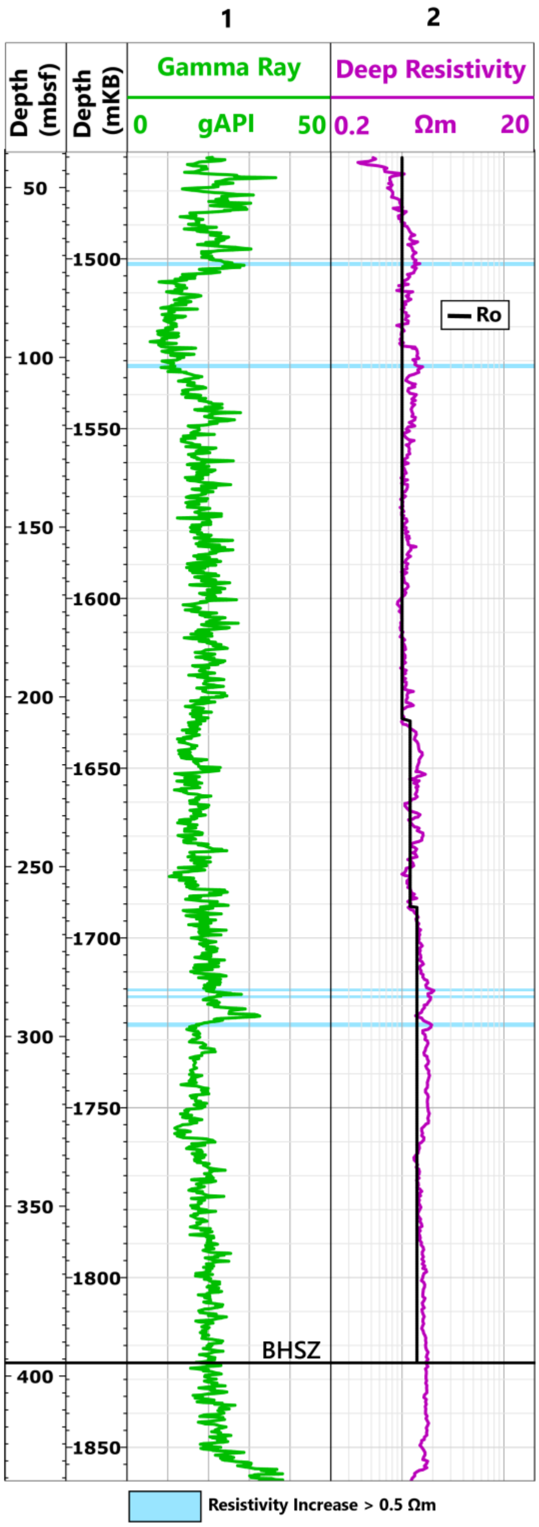

Figure 3 Well logs from Blackdragon-1 with an estimated R_o from 1-1.4 Ωm. The two depth tracks display depth in meters below seafloor (mbsf) and meters below rig floor (mKB). Track 1 displays gamma ray and Track 2 displays deep resistivity. R_o is 1 Ωm in the depth interval from 1429 -1636 mKB, 1.2 Ωm from 1636 - 1691 mKB and 1.4 Ωm below 1691 mKB. The highlighted intervals (blue) have resistivity increase > 0.5 Ωm that are interpreted as hydrate bearing intervals. This is a Category D well (Table 1). The BHSZ is estimated at 1825 mKB using a geothermal gradient of 34.9 C/km.

2.3 Gas hydrate categories

We categorize gas hydrate into four categories based on the increase in resistivity above R_o (Table 1) using the criteria modified from Majumdar et al. (2017). Category A is the highest category and has the largest increase in resistivity above R_o (5 Ωm) and the thickness of accumulations, whereas Category D is the lowest concentration and thickness of accumulation for hydrate out of the four categories. For example, we classify Yellowglen-1 (Figure 2) and Blackdragon-1 (Figure 3) wells as Category D hydrate, because the increase in resistivity is > 0.5 Ωm above background resistivity for a thickness of 2 m.

2.4 Seismic Interpretation

We interpret 18 3D seismic surveys covering a total area of 34130 km^2 with an aim of assessing the hydrate system in the North Carnarvon Basin. The 3D seismic surveys in the North Carnarvon Basin have a dominant frequency of 20-60 Hz, which results in a vertical resolution in the range 7-21 m assuming a velocity of 1700 m/s within the HSZ. Details on the inline and crossline spacing are available for each seismic survey in Table S1 of the Supplementary_Material pdf file.

To identify hydrate systems using seismic data, we first calculate the BHSZ for each seismic survey using the BHSZ calculation from the wells. To convert the BHSZ from depth to time in seismic data, we use an average interval velocity in shallow sediments available from the vertical seismic profiles (VSPs) in the well reports. We find that the average interval velocity within the HSZ varies from ~1590 m/s to ~1800 m/s in the North Carnarvon Basin. The BHSZ on the seismic surveys ranges from 50 – 600 ms two way travel time across the North Carnarvon Basin.

We look for BSRs, faults and the presence of gas to identify hydrate systems. We use zero phase American polarity where the seafloor is a positive amplitude reflection and the

BSR a negative amplitude reflection (Boswell et al., 2012; Hillman et al., 2017; Portnov et al., 2019). We use root-mean-square (RMS) amplitude maps to look for high amplitude areas near the estimated BHSZ that might indicate BSRs or free gas (Portnov et al., 2019). Then we manually inspect areas with high amplitudes. In the seismic data, we look for faults and chimneys that may act as pathways for fluid migration from the deep thermogenic reservoirs into the shallow sediments within HSZ.

3. Results and Discussion

Based on the well log interpretation from petroleum industry data, we find 52/120 wells (~43%) have evidence for natural gas hydrate in the North Carnarvon Basin (Figure 5 and Table 1). We also identify BSRs, gas chimneys, bright spots and faults in the North Carnarvon Basin using 3D seismic data.

Category	Description	Number of Wells
A	5 Ωm or above increase in resistivity above background resistivity for at least 10 m	0
B	2 Ωm or more (but less than 5 Ωm) increase in resistivity above background resistivity for at least 10 m, OR more than 5 Ωm increase above background resistivity but less than 10 m	2
C	0.5 Ωm to 2 Ωm increase in resistivity above background resistivity for at least 10 m, OR 2 Ωm or more (but less than 5 Ωm) increase in resistivity above background resistivity for less than 10 m	17
D	0.5 Ωm to 2 Ωm increase above background resistivity for less than 10 m	33
None		68
Total Wells		120

Table 1. Gas hydrate occurrence categorized based on the thickness of accumulation and increase in resistivity above background resistivity. The categories are modified from Majumdar et al., 2017.

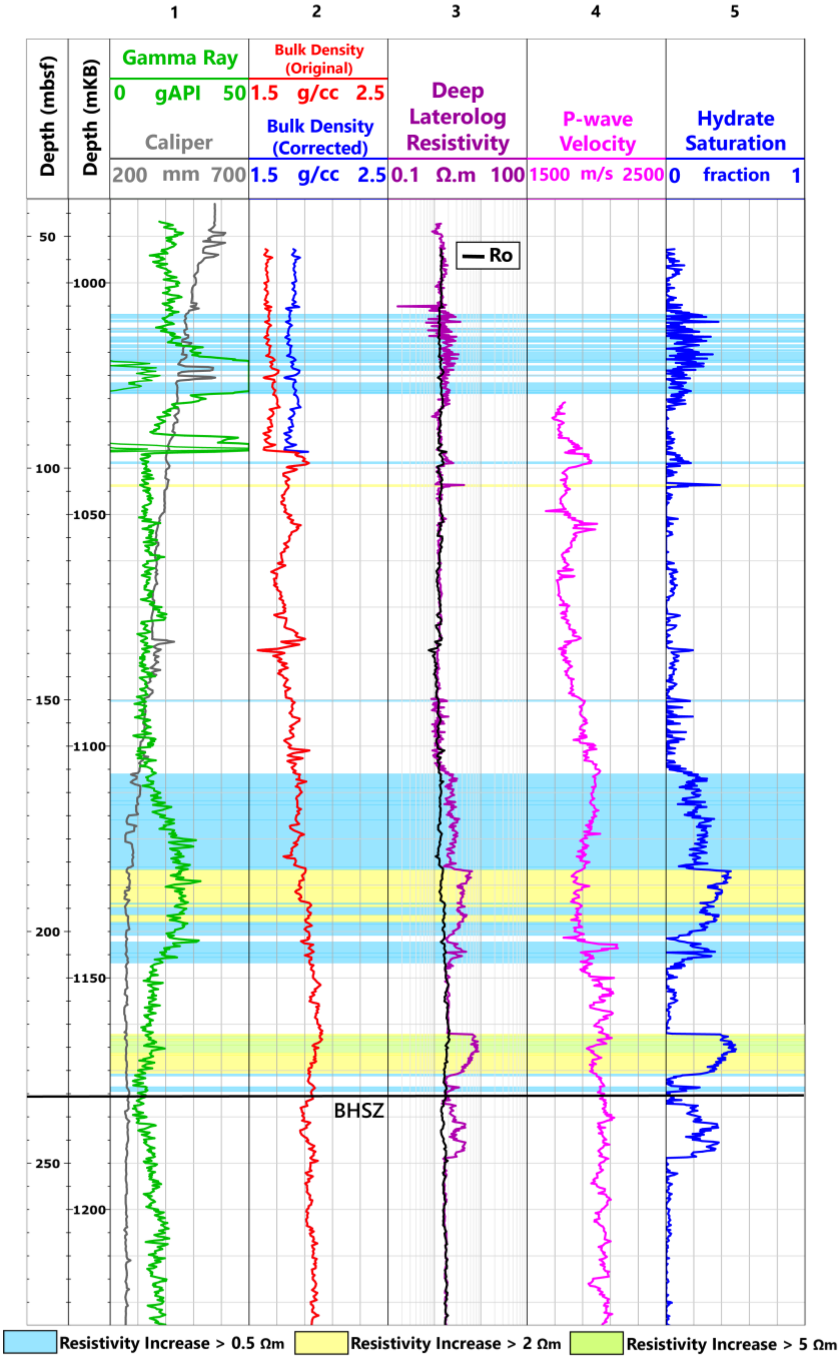

Figure 4 Well logs from Scarborough-2 with background resistivity (R_o) calculated using porosity from the bulk density log. The two depth tracks display depth in meters below sea floor (mbsf) and meters below kelly bushing (mKB) respectively. Track 1 displays gamma ray log (green) and caliper log (grey). Track 2 displays original bulk density (red) and corrected bulk density (blue). The bulk density log was corrected for borehole size in the shallow section. Track 3 displays the deep laterolog resistivity (purple) and R_o (black) using Archie's equation. Track 4 displays compressional velocity (pink). Track 5 displays hydrate saturation computed from Archie's equation (Equation (3)). The BHSZ is estimated to be at a depth of 1176 mKB using a geothermal gradient of 39.3 C/km. The hydrate bearing intervals are highlighted in blue (resistivity increase > 0.5 Ωm), yellow (resistivity increase > 2 Ωm) and green (resistivity increase > 5 Ωm). Based on the hydrate interpretation this well is classified as Category B hydrate.

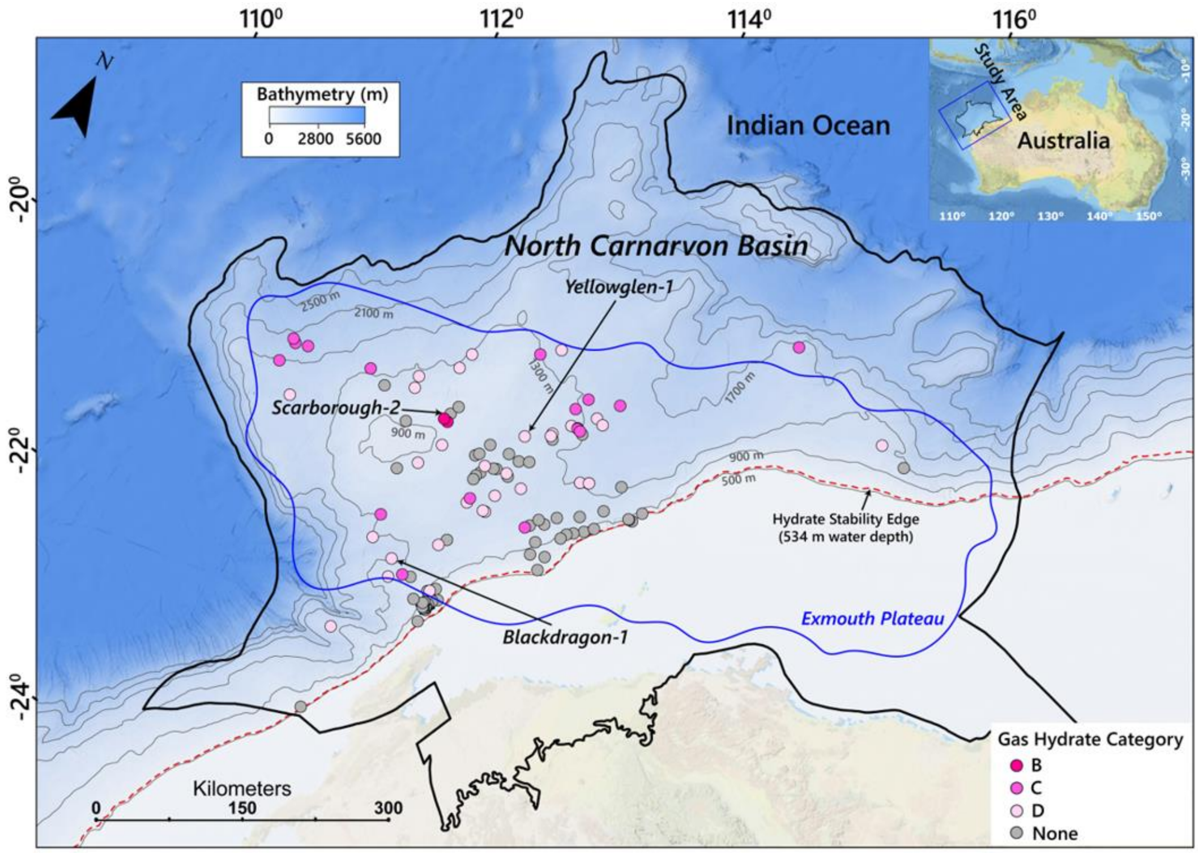

Figure 5 A map showing the location and gas hydrate category (Table 1) for wells in the North Carnarvon Basin.

3.1 Gas hydrate assessment using well data

We find that most of the wells in our dataset have increases in resistivity that are between 0.5 Ωm to 2 Ωm and are therefore in C or D Category (96%) (Table 1), showing that hydrate is present in low concentrations across the North Carnarvon Basin. For example, Yellowglen-1 and Blackdragon-1 wells (Figures 2 and 3) are both D Category wells. Both Yellowglen-1 and Blackdragon-1 wells host hydrate in thin intervals between 1470 to 1490 mKB and 1710 to 1730 mKB, respectively (Figure 2 and 3). Moreover, both Yellowglen-1 and Blackdragon-1 host hydrate present predominantly in carbonate ooze.

We also find that there are more hydrate accumulations in deeper water depths >1000 m (47/52 wells) in the North Carnarvon Basin (Figure 5 and Table 1). Interestingly, similar ratio of 118/124 gas hydrate wells were found in water depths > 1000 m in the Gulf of

Mexico from the results of Majumdar et al. (2017), though this result was not noted in the publication. This suggests a higher likelihood of hydrate in deeper water as compared to shallower water, and moreover, that this trend may persist across basins. This could simply be that a thicker HSZ increases the likelihood of hydrate, or more gas or organic matter may be present in deeper systems.

The two B Category wells (Scarborough-2 and Scarborough-3) are located ~4.5 km apart in the North Carnarvon Basin. Scarborough-2 has a full suite of well logs, which increases the confidence of our interpretation (Figure 4). In Scarborough-2, we interpret hydrate using laterolog resistivity by calculating R_o using Archie's equation (Figure 4). We choose m=1.85 for calculating R_o so that the R_o matches the laterolog resistivity in water saturated intervals (Ellis & Singer, 2007). We interpret hydrate in two different depth intervals from 1007 – 1050 mKB and below 1100 mKB (Figure 4). As observed on the resistivity log hydrate present from 1007 – 1050 mKB occupies discrete, thin lenses (Figure 4). Below 1100 mKB, hydrate is present in thicker layers consisting primarily of carbonate sediment (Figure 4). We do not observe an increase in compressional velocity below 1100 mKB, however, signifying that hydrate is present in relatively low saturation, likely less than 40% (Figure 4) (Yun et al., 2005). This agrees with our hydrate saturation calculation using n=2.3 in Equation (3) suggesting the saturation of hydrate ranging from ~13% to ~50% (Figure 4). In addition, we also observe an increase in resistivity above R_o below the BHSZ (Figure 4) from 1177 to 1188 mKB that we argue is more likely gas hydrate and not free gas. This is because compressional velocity reduces substantially with the presence of free gas, even a small amount of free gas (Murphy, 1984; Tõth et al., 2014). There is only a very slight increase in compressional velocity in this interval, however, suggesting that the increase in resistivity is more likely to be caused by hydrate at a saturation of 40% or less. (Figure 4). Moreover, the presence of gas hydrate below the BHSZ suggests the depth of the BHSZ is slightly underestimated at this well. For example, this might be the result of a slightly higher geothermal gradient. Here a small decrease in the geothermal gradient, from 39.3 C/km to 38 C/km, could account for the 15 m needed to lower the BHSZ.

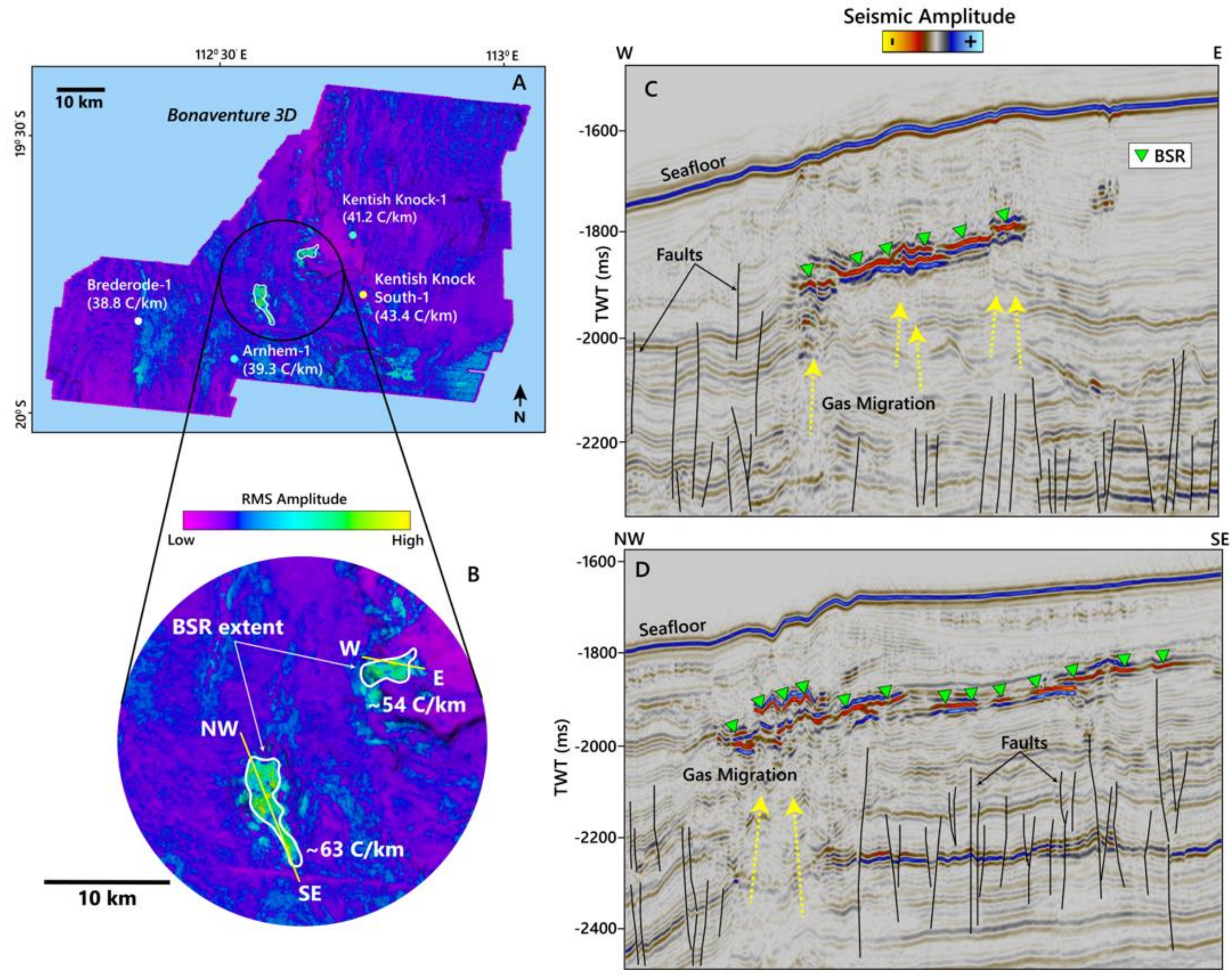

Figure 6 BSR interpretation in the Bonaventure 3D survey. (A) Map showing the location of BSRs and the four industry wells in Bonaventure 3D seismic survey. The location of the survey is shown in white polygon in Figure 1. The four wells in the survey area are plotted to indicate the background geothermal gradient (39 – 43° C/km) as computed from formation pressure tests. (B) RMS amplitude map at and near the BSR location with an offset of 300 ms below the seafloor and a time window of 100 ms capturing the inferred BHSZ for the survey area. The RMS amplitude map shows the BSR extent, and the geothermal gradient computed using BSR depth from the seafloor. (C) and (D) show seismic lines with interpreted BSR, gas chimneys and faults.

3.2 Connection to deep hydrocarbon reservoirs

We assess the potential connection between the presence of hydrate in a well and deeper hydrocarbon reservoirs using a similar approach as described by Cook et al. (2023). We place each well into two categories based on the information from the well reports: a hydrocarbon reservoir or no hydrocarbon reservoir. The well is categorized as a no hydrocarbon reservoir if the well does not have producible hydrocarbons. In the reports, the well may have been identified as a dry hole or a hole with only hydrocarbon shows (a small amount of hydrocarbon that is not producible). The well is categorized as having a hydrocarbon reservoir if it has producible hydrocarbons in the well reports.

In some cases, a well may be drilled at an angle (a deviated well) and the well location in the HSZ may be laterally offset from the well location in the hydrocarbon reservoir. We use available reservoir maps from the well reports to interpret if the well location in the HSZ still lies above the hydrocarbon reservoir. In our dataset, all 17 deviated wells still lie above the hydrocarbon reservoir.

<table>
<tr><th></th><th>Hydrate wells</th><th>Non-hydrate wells</th><th>Total number of wells used</th></tr>
<tr><td>Wells occurring above hydrocarbon reservoirs</td><td>30</td><td>47</td><td rowspan="2">110</td></tr>
<tr><td>No hydrocarbon reservoir</td><td>19</td><td>14</td></tr>
</table>

Table 2. Table shows number of hydrate vs non-hydrate wells occurring above a hydrocarbon reservoir and the total number of wells used for this analysis.

We use a total of 110 wells for hydrocarbon reservoir analysis. Based on the observation from data in Table 2, we consider the results in different ways to interpret the source of hydrate formation in the vicinity of wells in the North Carnarvon Basin. When no hydrocarbon reservoir is present below the HSZ (33 wells total), it is more likely that a well will be hydrate bearing (19/33 wells, Table 2). For these hydrate wells, the source of gas is most likely microbial in origin. When a hydrocarbon reservoir is present below the HSZ (77 wells total), it is less likely that any given well will be hydrate bearing (30/77, Table 2). This further implies that the source of gas in a hydrate system above a hydrocarbon reservoir is likely not thermogenic in origin.

For hydrate bearing wells (49 wells total), it is more likely that a hydrate well lies above a hydrocarbon reservoir (30/49 wells, Table 2). This could imply that there might be some connection between the occurrence of hydrate and the presence of thermogenic gas source below; however, it is also more likely that a non-hydrate well will lie above a hydrocarbon reservoir (47/61, Table 2). This implies that presence of hydrate is less likely to be connected to a thermogenic gas source below. All these observations, therefore, suggest that the hydrate system in the vicinity of the wells in the North Carnarvon Basin is most likely microbial in origin.

3.3 Hydrate interpretation using seismic data

Out of the 18 3D seismic surveys, we observe BSRs in only the Bonaventure 3D (Figure 1) seismic survey. Paganoni et al. (2019) previously reported the presence of these BSR-like features in the Bonaventure survey (Figure 1), and we agree the features described in Paganoni et al. (2019) are BSRs. At this location, the BSRs are associated with gas chimneys and faults implying a possible thermogenic source for the hydrate system (Figure 6).

We calculate the geothermal gradient locally using CSMHYD calculator with the identified BSRs as the BHSZ and compare it with the background geothermal gradient computed from the borehole formation pressure tests within the Bonaventure 3D survey. We find that the geothermal gradient within the extent of BSRs vary between ~54 – 63° C/km in contrast to the geothermal gradient of 39 – 43° C/km at the wells in the area (Figure 6). This elevated geothermal gradient is most likely the result of hot fluids advecting through the gas chimneys (Løseth et al., 2009).

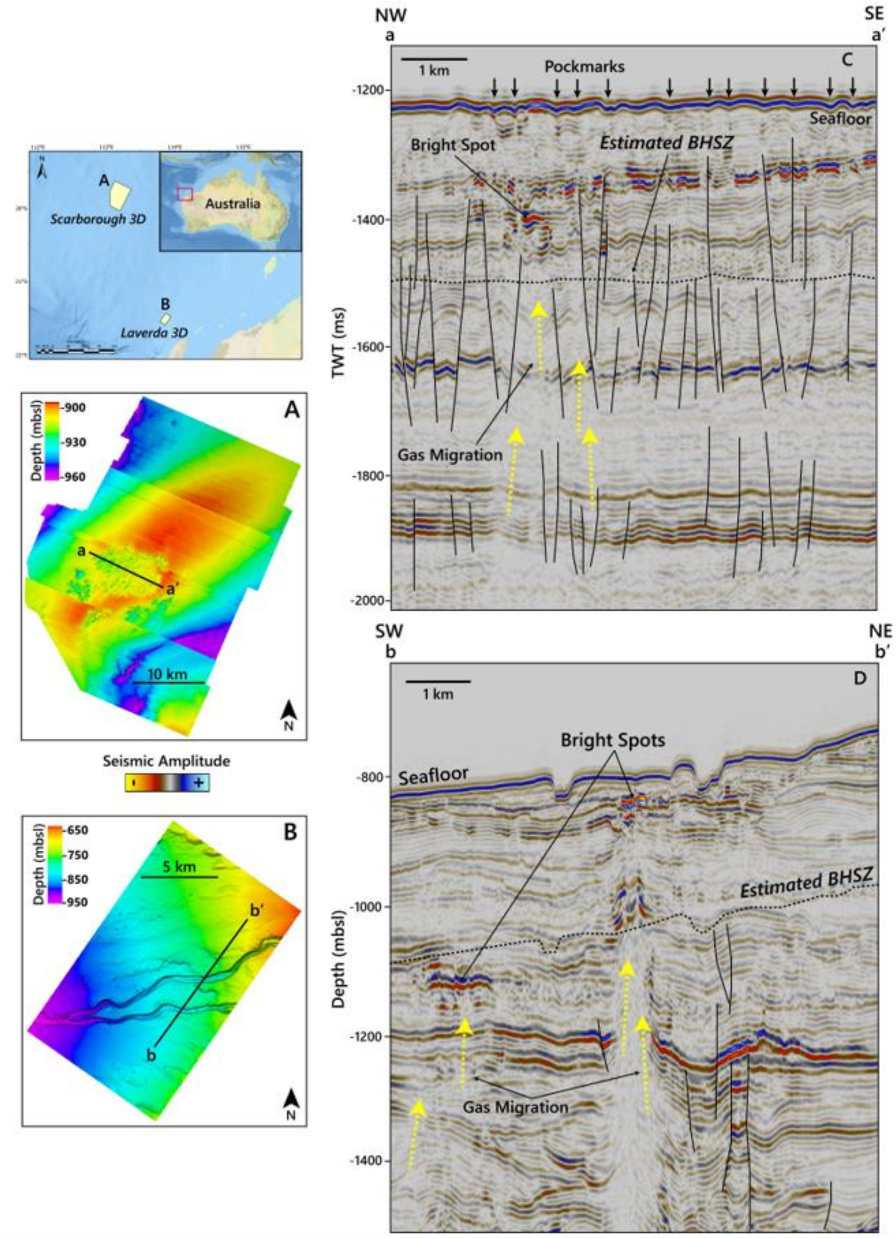

Figure 7 Examples from two different locations with gas chimneys breaching the estimated BHSZ in the North Carnarvon Basin. (A) Seafloor map from Scarborough 3D survey (B) Seafloor map from Laverda 3D survey (C) A seismic line from Scarborough 3D survey shows free gas rising up from the thermogenic reservoir into the HSZ and the presence of

bright spots and pockmarks that indicate the gas escaping out of the seafloor. (D) A gas chimney and associated bright spots in the Laverda 3D survey.

Because so few BSRs were observed in the 3D seismic datasets, we further investigate the frequency of gas chimneys feeding potential thermogenic hydrate systems by identifying gas chimneys breaching the inferred BHSZ in the North Carnarvon Basin. We find that only 17 chimneys breach the inferred BHSZ across all 3D seismic datasets (Figure 1). At these locations, thermogenic gas could source hydrate systems in the areas near the gas chimneys (for example Figure 7C and 7D). In addition, there is more evidence that may support the occurrence of gas migration: polygonal faults and bright spots associated with fault systems. Polygonal faults are pervasive across the seismic datasets across the North Carnarvon Basin (Zeng et al., (2022), see examples of polygonal faulting in Figures 6 and 7), however, bright spots are less commonly observed in the seismic data.

3.4 Inferred gas source for hydrate systems

We find different hydrate systems in the North Carnarvon Basin that have microbial and thermogenic gas sources, however, there is a strong bias towards hydrate systems with microbial source gas. As first suggested by Paganoni et al. (2019), we agree that hydrate systems at and near chimney features are more likely thermogenic in nature. In the 3D seismic data that covers an area of 34,000 km^2, we observe only 17 gas chimneys breaching the base of hydrate stability. In addition, there are locations with bright spots associated with faults in the North Carnarvon Basin, but they are not common. These observations suggest that the gas transport through faults may be low.

Hydrate was found in ~43% wells, however, most hydrate is in low concentrations in Categories C and D (Table 1). Low hydrate concentration that appears in different intervals throughout the HSZ (for examples see Figures 3 and 4) suggests that the source for that gas is more likely to be locally generated methane than from gas advection. Microbial methanogenesis of organic matter is likely sufficient to generate hydrate at low concentrations in the HSZ (Davie & Buffett, 2001; Malinverno, 2010; Xu & Ruppel, 1999), like the C and D Categories observed herein.

4. Conclusions

We use petroleum industry well logs and seismic data to understand the hydrate system in the North Carnarvon Basin, offshore Western Australia. We analyse 120 wells and find ~43% wells with evidence of hydrate. We observe that most of the hydrate is present in low concentrations. We also observe most hydrate accumulations are distributed throughout the HSZ and are not concentrated near the BHSZ. Moreover, we find that hydrate bearing wells do not likely occur above a hydrocarbon reservoir implying that the gas source for hydrate is not likely thermogenic in origin further implying a microbial source for gas. On the seismic data, we observe BSRs only in one seismic survey out of 18 3D seismic surveys. We also observe only 17 gas chimneys on seismic data breaching the inferred BHSZ. Moreover, there are few locations with bright spots associated with faults implying low gas transport through faults. These observations signify a weak thermogenic gas source for hydrate formation near the vicinity of such a low number of gas chimneys, BSRs and bright spots. In contrast, there are more well locations providing a strong evidence for a predominant microbial gas source for hydrate in the North Carnarvon Basin.

Acknowledgements

The authors would like to thank Dr. Ben Clennell, CSIRO, Australia for providing valuable information about using the NOPIMS and WAPIMS databases. We would also like to thank Aditya Kumar and Rene Castillo for helping with data loading and software. We would also thank Geoscience Australia for providing well and seismic data from NOPIMS and WAPIMS databases to work on this project. Finally, we thank Schlumberger for providing Techlog and Petrel software at The Ohio State University.

Funding: This work was supported by National Science Foundation [Award number 1752882].

Author Contributions

Fawz Naim: Data Curation, Formal Analysis, Investigation, Methodology, Software, Writing-original draft; **Ann E Cook**: Conceptualization, Investigation, Funding Acquisition, Methodology, Resources, Supervision, Writing-original draft, review & editing.

Data Availability Statement

The well data used in this project can be downloaded from NOPIMS (https://www.ga.gov.au/nopims) database. The seismic data is available through Geoscience Australia and the seismic survey locations can be viewed on WAPIMS (https://wapims.dmp.wa.gov.au/WAPIMS/) database. All the details related to the well data analysis is available in the Supplementary_Material spreadsheet. Also, the updated bathymetry map, HSZ thickness map and seismic data spatial resolution are available in the Supplementary_Material pdf.

References

Anderson, B., Hancock, S., Wilson, S., Enger, C., Collett, T., Boswell, R., & Hunter, R. (2011). Formation pressure testing at the Mount Elbert Gas Hydrate Stratigraphic Test Well, Alaska North Slope: Operational summary, history matching, and interpretations. *Marine and Petroleum Geology*, *28*(2). https://doi.org/10.1016/j.marpetgeo.2010.02.012

Archie, G. E. (1942). The electrical resistivity log as an aid in determining some reservoir characteristics. *Transactions of the AIME*.

Barrett, B. J., Hodgson, D. M., Jackson, C. A. L., Lloyd, C., Casagrande, J., & Collier, R. E. L. (2021). Quantitative analysis of a footwall-scarp degradation complex and syn-rift stratigraphic architecture, Exmouth Plateau, NW Shelf, offshore Australia. *Basin Research*, *33*(2). https://doi.org/10.1111/bre.12508

Bellefleur, G., Riedel, M., Brent, T., Wright, F., & Dallimore, S. R. (2007). Implication of seismic attenuation for gas hydrate resource characterization, Mallik, Mackenzie Delta, Canada. *Journal of Geophysical Research: Solid Earth*, *112*(10). https://doi.org/10.1029/2007JB004976

Boswell, R., & Collett, T. S. (2011). Current perspectives on gas hydrate resources. In *Energy and Environmental Science* (Vol. 4, Issue 4). https://doi.org/10.1039/c0ee00203h

Boswell, R., Collett, T. S., Frye, M., Shedd, W., McConnell, D. R., & Shelander, D. (2012). Subsurface gas hydrates in the northern Gulf of Mexico. *Marine and Petroleum Geology*, *34*(1). https://doi.org/10.1016/j.marpetgeo.2011.10.003

Boswell, R., Shipp, C., Reichel, T., Shelander, D., Saeki, T., Frye, M., Shedd, W., Collett, T. S., & McConnell, D. R. (2016). Prospecting for marine gas hydrate resources. *Interpretation*, *4*(1). https://doi.org/10.1190/INT-2015-0036.1

Boyer, T. P., Garcia, H. E., Locarnini, R. A., Zweng, M. M., Mishonov, A. V., Reagen, J. R., Weathers, K. A., Baranova, O. K., Seidov, D., & Smolyar, I. V. (2018). *World Ocean Atlas 2018*. WOA 2018 Data. NOAA National Centers for Environmental Information. Dataset. https://www.ncei.noaa.gov/archive/accession/NCEI-WOA18.

Bradshaw, M. T., Bradshaw, J., Murray, A. P., Needham, D. J., Spencer, L., Summons, R. E., Wilmot, J., & Winn, S. (1994). Petroleum systems in West Australian basins. In *The sedimentary basins of Western Australia* (pp. 43–53).

Brooks, J. M., Kennicutt, M. C., Fay, R. R., McDonald, T. J., & Sassen, R. (1984). Thermogenic gas hydrates in the Gulf of Mexico. *Science*, *225*(4660). https://doi.org/10.1126/science.225.4660.409

Cartwright, J., James, D., & Bolton, A. (2003). The genesis of polygonal fault systems: A review. *Geological Society Special Publication*, *216*. https://doi.org/10.1144/GSL.SP.2003.216.01.15

Cartwright, J., & Lonergan, L. (1997). Seismic expression of layer-bound fault systems of the Eromanga and North Sea Basins. *Exploration Geophysics*, *28*(3). https://doi.org/10.1071/EG997323

Claypool, G. E., & Kvenvolden, K. A. (1983). Methane and other hydrocarbon gases in marine sediment. *Annual Review of Earth and Planetary Sciences. Vol. 11*. https://doi.org/10.1146/annurev.ea.11.050183.001503

Collett, T.S., Boswell, R., Cochran, J. R., Kumar, P., Lall, M., Mazumdar, A., Ramana, M. V., Ramprasad, T., Riedel, M., Sain, K., Sathe, A. V., & Vishwanath, K. (2014). Geologic implications of gas hydrates in the offshore of India: Results of the National Gas Hydrate Program Expedition 01. *Marine and Petroleum Geology*, *58*(PA). https://doi.org/10.1016/j.marpetgeo.2014.07.021

Collett, Timothy S., Boswell, R., Waite, W. F., Kumar, P., Roy, S. K., Chopra, K., Singh, S. K., Yamada, Y., Tenma, N., Pohlman, J., & Zyrianova, M. (2019). India National Gas Hydrate Program Expedition 02 Summary of Scientific Results: Gas hydrate systems along the eastern continental margin of India. *Marine and Petroleum Geology*, *108*, 39–142. https://doi.org/10.1016/j.marpetgeo.2019.05.023

Collett, Timothy S, Johnson, A. H., Knapp, C. C., & Boswell, R. (2009). Natural gas hydrates: A review. *AAPG Memoir*.

Cook, A. E., Portnov, A., Heber, R. C., Vadakkepuliyambatta, S., & Bünz, S. (2023). Widespread subseafloor gas hydrate in the Barents Sea and Norwegian Margin. *Earth and Planetary Science Letters*, *604*, 117993. https://doi.org/10.1016/j.epsl.2023.117993

Cowley, R., & O'Brien, G. W. (2000). IDENTIFICATION AND INTERPRETATION OF LEAKING HYDROCARBONS USING SEISMIC DATA:A COMPARATIVE MONTAGE OF EXAMPLES FROM THE MAJOR FIELDS IN AUSTRALIA'S NORTHWEST SHELF AND GIPPSLAND BASIN. *The APPEA Journal*, *40*(1). https://doi.org/10.1071/aj99008

Davie, M. K., & Buffett, B. A. (2001). A numerical model for the formation of gas hydrate below the seafloor. *Journal of Geophysical Research: Solid Earth*, *106*(B1). https://doi.org/10.1029/2000jb900363

Dickens, G. R. (2003). Rethinking the global carbon cycle with a large, dynamic and microbially mediated gas hydrate capacitor. *Earth and Planetary Science Letters*, *213*(3–4). https://doi.org/10.1016/S0012-821X(03)00325-X

Ellis, D. V., & Singer, J. M. (2007). Well Logging for Earth Scientists. In *Well Logging for Earth Scientists*. https://doi.org/10.1007/978-1-4020-4602-5

Evans, T. R., & Coleman, N. C. (1974). North Sea geothermal gradients. *Nature*, *247*(5435). https://doi.org/10.1038/247028a0

Exon, N. F., & Willcox, J. B. (1980). THE EXMOUTH PLATEAU: STRATIGRAPHY, STRUCTURE, AND PETROLEUM POTENTIAL. *Bulletin - Bureau of Mineral Resources, Geology and Geophysics (Australia)*, *199*.

Flemings, P. B., Phillips, S. C., Boswell, R., Collett, T. S., Cook, A. E., Dong, T., Frye, M., Goldberg, D. S., Guerin, G., Holland, M. E., Jang, J., Meazell, K., Morrison, J., O'Connell, J. I., Petrou, E. G., Pettigrew, T., Polito, P. J., Portnov, A., Santra, M., … You, K. (2020). Pressure coring a Gulf of Mexico deep-water turbidite gas hydrate reservoir: Initial results from the University of Texas-Gulf of Mexico 2-1 (UT-GOM2-1) Hydrate Pressure Coring Expedition. *AAPG Bulletin*, *104*(9). https://doi.org/10.1306/05212019052

Fujii, T., Suzuki, K., Takayama, T., Tamaki, M., Komatsu, Y., Konno, Y., Yoneda, J., Yamamoto, K., & Nagao, J. (2014). Geological setting and characterization of a methane hydrate reservoir distributed at the first offshore production test site on the Daini- Atsumi Knoll in the eastern Nankai Trough, Japan. *Marine and Petroleum Geology*, *66*. https://doi.org/10.1016/j.marpetgeo.2015.02.037

Gallagher, S. J., Fulthorpe, C. S., Bogus, K., Auer, G., Baranwal, S., Castañeda, I. S., Christensen, B. A., De Vleeschouwer, D., Franco, D. R., Groeneveld, J., Gurnis, M., Haller, C., He, Y., Henderiks, J., Himmler, T., Ishiwa, T., Iwatani, H., Jatiningrum, R. S., Kominz, M. A., … Zhang, W. (2017). *Expedition 356 summary* (Vol. 356, Issue February). https://doi.org/10.14379/iodp.proc.356.101.2017

Goldberg, D., Kleinberg, R. L., Weinberger, J. L., Malinverno, A., McLellan, P. J., & Collett, T. S. (2010). 16. Evaluation of Natural Gas-Hydrate Systems Using Borehole Logs. In *Geophysical Characterization of Gas Hydrates*. https://doi.org/10.1190/1.9781560802197.ch16

Haacke, R. R., Westbrook, G. K., & Hyndman, R. D. (2007). Gas hydrate, fluid flow and free gas: Formation of the bottom-simulating reflector. *Earth and Planetary Science Letters*, *261*(3–4). https://doi.org/10.1016/j.epsl.2007.07.008

Haq, B. U., Von Rad, U., O'Connell, S., & et al. (1990). Proceedings of the Ocean Drilling Program, 122 Initial Reports. In *Proceedings of the Ocean Drilling Program, 122 Initial Reports*. https://doi.org/10.2973/odp.proc.ir.122.1990

Heggland, R. (1998). Gas seepage as an indicator of deeper prospective reservoirs. A study based on exploration 3D seismic data. *Marine and Petroleum Geology*, *15*(1). https://doi.org/10.1016/S0264-8172(97)00060-3

Helgerud, M. B., Dvorkin, J., Nur, A., Sakai, A., & Collett, T. (1999). Elastic-wave velocity in marine sediments with gas hydrates: Effective medium modeling. *Geophysical Research Letters*. https://doi.org/10.1029/1999GL900421

Hillman, J. I. T., Cook, A. E., Daigle, H., Nole, M., Malinverno, A., Meazell, K., & Flemings, P. B. (2017). Gas hydrate reservoirs and gas migration mechanisms in the Terrebonne Basin, Gulf of Mexico. *Marine and Petroleum Geology*, *86*. https://doi.org/10.1016/j.marpetgeo.2017.07.029

Hillman, J. I. T., Crutchley, G. J., & Kroeger, K. F. (2020). Investigating the role of faults in fluid migration and gas hydrate formation along the southern Hikurangi Margin, New Zealand. *Marine Geophysical Research*, *41*(1). https://doi.org/10.1007/s11001-020-09400-2

Holbrook, W. S., Hoskins, H., Wood, W. T., Stephen, R. A., & Lizarralde, D. (1996). Methane hydrate and free gas on the Blake Ridge from vertical seismic profiling. *Science*. https://doi.org/10.1126/science.273.5283.1840

Hui, G., Li, S., Guo, L., Zhang, G., Gong, Y., Somerville, I. D., Zhang, Y., Zheng, Q., & Zang, Y. (2016). Source and accumulation of gas hydrate in the northern margin of the South China Sea. *Marine and Petroleum Geology*, *69*. https://doi.org/10.1016/j.marpetgeo.2015.10.009

Imbert, P., & Ho, S. (2012). Seismic-scale funnel-shaped collapse features from the Paleocene-Eocene of the North West Shelf of Australia. *Marine Geology*, *332–334*. https://doi.org/10.1016/j.margeo.2012.10.010

Kvenvolden, K. A. (1988). Methane hydrate - A major reservoir of carbon in the shallow geosphere? *Chemical Geology*, *71*(1–3). https://doi.org/10.1016/0009-2541(88)90104-0

Kvenvolden, K. A. (2002). Methane hydrate in the global organic carbon cycle. *Terra Nova*. https://doi.org/10.1046/j.1365-3121.2002.00414.x

Lee, M. W., & Collett, T. S. (2011). In-situ gas hydrate hydrate saturation estimated from various well logs at the Mount Elbert Gas Hydrate Stratigraphic Test Well, Alaska North Slope. *Marine and Petroleum Geology*. https://doi.org/10.1016/j.marpetgeo.2009.06.007

Ligtenberg, J. H. (2003). Unravelling the petroleum system by enhancing fluid migration paths in seismic data using a neural network based pattern recognition technique. *Geofluids*, *3*(4). https://doi.org/10.1046/j.1468-8123.2003.00072.x

Locarnini, R. A., Mishonov, A. V., Baranova, O. K., Boyer, T. P., Zweng, M. M., Garcia, H. E., Reagan, J. R., Seidov, D., Weathers, K. W., Paver, C. R., & Smolyar, I. V. (2018). World Ocean Atlas 2018, Volume 1: Temperature. *NOAA Atlas NESDIS 81*, *1*(July).

Løseth, H., Gading, M., & Wensaas, L. (2009). Hydrocarbon leakage interpreted on seismic data. *Marine and Petroleum Geology*, *26*(7). https://doi.org/10.1016/j.marpetgeo.2008.09.008

Majumdar, U., Cook, A. E., Scharenberg, M., Burchwell, A., Ismail, S., Frye, M., & Shedd, W. (2017). Semi-quantitative gas hydrate assessment from petroleum industry well logs in the northern Gulf of Mexico. *Marine and Petroleum Geology*, *85*. https://doi.org/10.1016/j.marpetgeo.2017.05.009

Malinverno, A. (2010). Marine gas hydrates in thin sand layers that soak up microbial methane. *Earth and Planetary Science Letters*, *292*(3–4). https://doi.org/10.1016/j.epsl.2010.02.008

Maslin, M., Owen, M., Betts, R., Day, S., Jones, T. D., & Ridgwell, A. (2010). Gas hydrates: Past and future geohazard? *Philosophical Transactions of the Royal Society A: Mathematical, Physical and Engineering Sciences*, *368*(1919). https://doi.org/10.1098/rsta.2010.0065

Miller, P., Dasgupta, S., & Shelander, D. (2012). Seismic imaging of migration pathways by advanced attribute analysis, Alaminos Canyon 21, Gulf of Mexico. *Marine and Petroleum Geology*, *34*(1). https://doi.org/10.1016/j.marpetgeo.2011.09.005

Murphy, W. F. (1984). Acoustic measures of partial gas saturation in tight sandstones. *Journal of Geophysical Research: Solid Earth*, *89*(B13). https://doi.org/10.1029/jb089ib13p11549

Pearson, C. F., Halleck, P. M., McGuire, P. L., Hermes, R., & Mathews, M. (1983). Natural gas hydrate deposits: A review of in situ properties. *Journal of Physical Chemistry*. https://doi.org/10.1021/j100244a041

Peters, K. E., & Nelson, P. H. (2012). Criteria to determine borehole formation temperatures for calibration of basin models. *SEPM Special Publication*, *103*.

Phillips, S. C., Flemings, P. B., Holland, M. E., Schultheiss, P. J., Waite, W. F., Jang, J., Petrou, E. G., & Hammon, H. (2020). High concentration methane hydrate in a silt reservoir from the deep-water Gulf of Mexico. *AAPG Bulletin*, *104*(9). https://doi.org/10.1306/01062018280

Portnov, A., Cook, A. E., Sawyer, D. E., Yang, C., Hillman, J. I. T., & Waite, W. F. (2019).

Clustered BSRs: Evidence for gas hydrate-bearing turbidite complexes in folded regions, example from the Perdido Fold Belt, northern Gulf of Mexico. *Earth and Planetary Science Letters*, *528*. https://doi.org/10.1016/j.epsl.2019.115843

Regional Geology of the Northern Carnarvon Basin. (2022).

Ruppel, C., & Kessler, J. (2017). The interaction of climate change and methane hydrates. In *Reviews of Geophysics*. https://doi.org/10.1002/2016RG000534

Ryu, B. J., Riedel, M., Kim, J. H., Hyndman, R. D., Lee, Y. J., Chung, B. H., & Kim, I. S. (2009). Gas hydrates in the western deep-water Ulleung Basin, East Sea of Korea. *Marine and Petroleum Geology*, *26*(8). https://doi.org/10.1016/j.marpetgeo.2009.02.004

Sheriff, R. E. (1975). FACTORS AFFECTING SEISMIC AMPLITUDES. *Geophysical Prospecting*, *23*(1). https://doi.org/10.1111/j.1365-2478.1975.tb00685.x

Shipley, T. H. (1979). Seismic evidence for widespread possible gas hydrate horizons on continental slopes and rises. In *American Association of Petroleum Geologists, Bulletin* (Vol. 63, Issue 12). https://doi.org/10.1306/2f91890a-16ce-11d7-8645000102c1865d

Sloan, E. D., & Koh, C. A. (2007). Clathrate hydrates of natural gases, thrid edition. In *Clathrate Hydrates of Natural Gases, Third Edition*. https://doi.org/10.1201/9781420008494

Snowdon, L. R., & Meyers, P. A. (1992). Source and maturity of organic matter in sediments and rocks from Sites 759, 760, 761, and 764 (Wombat Plateau) and Sites 762 and 763 (Exmouth Plateau). *Proc. Scientific Results, ODP, Leg 122, Exmouth Plateau*. https://doi.org/10.2973/odp.proc.sr.122.131.1992

Takahashi, H., Fercho, E., & Dallimore, S. R. (2005). Drilling and operations overview of the Mallik 2002 Production Research Well Program. *Geological Survey of Canada Bulletin*, *585*.

Tõth, Z., Spiess, V., Mogollõn, J. M., & Jensen, J. B. (2014). Estimating the free gas content in Baltic Sea sediments using compressional wave velocity from marine seismic data. *Journal of Geophysical Research: Solid Earth*, *119*(12). https://doi.org/10.1002/2014JB010989

Tsuji, Y., Fujii, T., Hayashi, M., Kitamura, R., Nakamizu, M., Ohbi, K., Saeki, T., Yamamoto, K., Namikawa, T., Inamori, T., Oikawa, N., Shimizu, S., Kawasaki, M., Nagakubo, S., Matsushima, J., Ochiai, K., & Okui, T. (2009). Methane-hydrate Occurrence and Distribution in the Eastern Nankai Trough, Japan: Findings of the Tokai-oki to Kumano-nada Methane-hydrate Drilling Program. *Natural Gas Hydrates - Energy Resource Potential and Associated Geologic Hazards: AAPG Memoir 89*, *c*, 228–246. https://doi.org/10.1306/13201103M893129

Xu, W., & Ruppel, C. (1999). Predicting the occurrence, distribution, and evolution of methane gas hydrate in porous marine sediments. *Journal of Geophysical Research: Solid Earth*, *104*(B3). https://doi.org/10.1029/1998jb900092

Yun, T. S., Francisca, F. M., Santamarina, J. C., & Ruppel, C. (2005). Compressional and shear wave velocities in uncemented sediment containing gas hydrate. *Geophysical Research Letters*. https://doi.org/10.1029/2005GL022607

Zeng, Z., Zhu, H., Yang, X., & Cao, X. (2022). Three-dimensional seismic analysis of a polygonal fault system (PFS) in the Northern Carnarvon Basin, Australia: Implications for fluid flow migration and gas hydrate system. *Journal of Petroleum Science and Engineering*, *215*. https://doi.org/10.1016/j.petrol.2022.110602